In situ synchrotron diffraction investigation of morphotropic Pb[Zr$_{1-x}$Ti$_x$]O$_3$ under an applied electric field

Kristin A. Schönau,[1,*] Michael Knapp,[1,2] Hans Kungl,[3] Michael J. Hoffmann,[3] and Hartmut Fuess[1]

[1]*Materials Science, Darmstadt University of Technology, D-64287 Darmstadt, Germany*

[2]*CELLS, P.O. Box 68, 08193 Barcelona, Spain*

[3]*Institute of Ceramics in Mechanical Engineering, University of Karlsruhe, D-76131 Karlsruhe, Germany*

For understanding the reaction of the domain structure and crystallographic structure of ferroelectric lead zirconate titanate, Pb[Zr$_{1-x}$Ti$_x$]O$_3$, to an applied electric field and its high piezoelectric properties for compositions in the vicinity of the morphotropic phase boundary (MPB), investigations of structural changes under *in situ* conditions are of great importance. As we have shown in recent studies [L. A. Schmitt *et al.*, J. Appl. Phys. **101**, 074107 (2007); K. A. Schönau *et al.*, Phys. Rev. B **75**, 184117 (2007)] the domain structure miniaturizes at the MPB. This nanodomain structure and its stability field are crucial for the character of the poling behavior of the material. *In situ* electric field synchrotron powder diffraction studies across the entire compositional range of the MPB show changes in phase fractions, domain structure, and phase transitions under electric field dependent on the nanodomain content. For a certain range of tetragonal c/a-ratio the nanodomains are stabilized, straining tetragonal microdomains under electric field, while with further decreasing c/a-ratio at higher Zr contents they are transformed into a structure associable with rhombohedral microdomains.

I. INTRODUCTION

The solid solution lead zirconate titanate, Pb[Zr$_{1-x}$Ti$_x$]O$_3$, (PZT) is a widely used ferroelectric material. In particular, samples of compositions at the morphotropic phase boundary (MPB) between the tetragonal (*P4mm*) and rhombohedral (*R3m*) phase fields are implemented in industrial applications, as they depict highest dielectric properties and strain values under electric field.[1,2] In spite of many investigations in recent years the origin of these effects is still controversial. Coexistence of both tetragonal and rhombohedral phases[3] has been discussed as well as the presence of a monoclinic *Cm* phase,[4] forming a two-dimensional ferroelectric in which a polarization rotation was feasible without a change of crystallographic structure.[5] Another model was proposed by Jin *et al.*[6] for the interpretation of observed macroscopic features in PMN-PT. The authors associated the high strain with a reorientation of nanodomain structures. Lately, Rao and Wang[7] used computer simulations to show that within a heavily stressed tetragonal 90° domain wall a rhombohedral phase may be induced under the application of an electric field in pseudocubic $[111]_c$ direction.

Recent investigations on undoped PZT of morphotropic composition demonstrated the presence of nanodomain structures.[8] These nanodomains can directly be correlated to features in x-ray patterns previously interpreted as a monoclinic phase.[9] As the width of these nanodomains is very small, coherence effects influence diffraction. The true internal symmetry may not be determined, analogously to diffraction on nanodomains in relaxor materials, as theoretical calculations by Wang and others[6,10,11] using diffraction theory show. As the macroscopically observed symmetry in diffraction can be described as *Cm*, martensitic theory predicts[6,12,13] that the internal symmetry of nanodomains present at the MPB in the PZT solid solution system is likely to be rhombohedral. The resulting possible phase coexistence of tetragonal microdomains and nanodomain structures is underlined

by computational studies[14] showing a mosaic domain microstructure of rhombohedral nanodomains beside tetragonal microdomains for compositions in the vicinity of the MPB in PZT.

The macroscopic strain measured under electric field is attributed to contributions of both the reorientation of the domains and the stretching of the unit cell. Generally, interpretation is based on an idealized structure and a discrimination between both effects is difficult, as e.g., the reorientation of the domains under field can as well stress the unit cells.[15] High-resolution x-ray diffraction pattern may, however, provide this additional information on the reaction of the microstructure to a poling process and under electric cycling.[2,15]

Tetragonal ferroelectric materials contain two different types of domain structures - between domains the polarization vector changes in almost right angle, the boundary is known as 90° domain walls, and 180° domain walls separate domains which have antiparallel polarization vectors.[16] The rearrangement of domain configurations separated by 180° domain walls therefore only plays a minor role in terms of texture visible in x-ray diffraction experiments, but contributes to the microscopic strain through elongation or contraction of the unit cell with respect to their orientation to the electric field. The change in spatial orientation of domains with 90° domain walls significantly contributes to the texture effects and also contribution to microscopic strain is observed.[2,17,18]

So far most of the *in situ* diffraction experiments on polycrystalline ceramics have been conducted recording and analyzing single reflections or pairs of reflections. Domain switching was calculated from changes in integral intensities and lattice changes from peak shifts.[15,19–26] Besides the work of Menou *et al.*,[21] all these studies focused on donor doped material. For compositions close to the MPB mostly the model of a coexistence of a tetragonal and rhombohedral phase[26] or a tetragonal and monoclinic phase[23] was assumed and analyzes concentrated on the measurement of the

pseudocubic $\{111\}_c$ and $\{200\}_c$ reflections assuming constant phase contents. To extract information on texture changes between poled and unpoled single phase tetragonal PZT samples Jones *et al.*[18] applied Rietveld refinement using a spherical harmonics model.

Apart from texture analysis the Rietveld method provides a powerful tool to supply structural information on individual phases in a multiphase solid, deriving information from the fit of the entire diffraction pattern. As the discussion on possible phase transitions and polarization rotation in morphotropic material as origin for the high piezoelectric effect is vivid,[27] we have undertaken a full pattern analysis of *in situ* powder diffraction data of undoped PZT of morphotropic compositions. The application of the Rietveld method not only allows for the detailed extraction of structural data but also enables monitoring of changes in phase content and possible phase transitions under electric cycling not possible using single peak fits. This may provide a model for the behavior of nanodomain structures under electric field.

II. EXPERIMENT

A set of samples ranging across the entire compositional range of the MPB was subjected to *in situ* synchrotron x-ray powder diffraction.

Samples were prepared by a mixed-oxide route[28] with Zr/Ti contents of 60/40, 57.5/42.5, 56/44, 55/45, 54.5/45.5, 54/46, 53.5/46.5, 53/47, 52.5/47.5, and 52/48. Powders were pressed uniaxially into cylindrical pellets of 12 mm in diameter at 17.7 MPa, followed by cold isostatic pressing at 400 MPa. The pellets were then sintered at 1050 °C for 6 h with a heating rate of 2 °C min^{-1} up to this temperature. Analysis of the grain size was conducted using scanning electron microscopy (SEM) (Zeiss DSM 962, working at 25 kV) on polished and then chemically etched samples. The average grain size was determined to be around 7 μm (Ref. 36) using the linear intercept method with the program LINCE 2.31D.[29]

Macroscopic strain was measured in a custom made device equipped with a one-point mounting sample holder and strain recording system based on a linear variable displacement transducer (LVDT). Both the application of electric fields from a bipolar high voltage source (FUG) and the recording of strain data were controlled by a LABVIEW software. Frequency of all electrical cycles was 5 mHz. Slices, cut from cylindrical ceramic bodies (9 mm in diameter and 7 mm in height) and subsequently ground and polished to a thickness of 1 mm, were used as samples. Electrical contact was provided by silver paint electrodes (Gwent) fired on at 600 °C. Poling of the samples was accomplished by bipolar electrical cycling. Starting with maximum electric fields of 1 kV/mm the maximum field in subsequent cycles was increased in four steps to 4 kV/mm. Four bipolar cycles were applied at each field level. The strain under bipolar cycling at 4 kV/mm, as evaluated in this work, was recorded immediately after this poling procedure.

In situ electric field synchrotron x-ray powder diffraction measurements were conducted at the beamline B2, Hasylab Hamburg, Germany.[30] A special transmission setup was con-
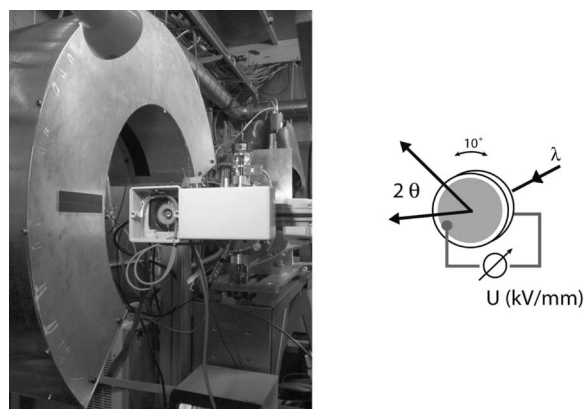
FIG. 1. Setup for *in situ* electric field measurements at beamline B2, HASYLAB Hamburg, Germany. The sample is oscillated 10° around beam direction. Electric field is applied in beam direction. Data acquisition is performed using the position-sensitive image-plate detector (OBI) (Ref. 31) or alternatively a scintillation single counter with analyzing crystal (Ref. 30).

structed to apply a static field in beam direction, oscillating the sample about 10° around the beam as well as field direction to improve statistics (Fig. 1). Polycrystalline pellets were cut and polished to a thickness of 50–70 μm. Pt electrodes ($\varnothing$8 mm, ~15 nm thickness) were sputtered onto both sides. Measurements were performed in high-resolution setup using a scintillation single counter and analyzing crystal with a step size of 0.004° for *ex situ* investigation, and using a position-sensitive image-plate detector (OBI)[31] for all *in situ* electric field measurements at an incident wavelength of $\lambda \sim 0.05$ nm. Voltage was applied statically in bipolar cycles of up to 4 kV/mm.

Diffraction data were analyzed using the general structure analysis program GSAS.[32] The data sets were fitted using a Thompson-Cox-Hastings pseudo-Voigt function[33] and linear interpolation of fixed background points. To partly accommodate the anisotropy in the full width at half maximum caused by the domain structure, the profiles were additionally varied using the GSAS incorporated generalized model for anisotropic peak broadening by Stephens.[34] A March-Dollase (MD) model[35] was applied to account for texture in the tetragonal phase. Despite recent criticism on the applicability of this model,[18] it may be used in our case, as the influence of texture perpendicular to the beam direction is minimized through the oscillating setup and no angle dependent texture analysis is performed. Therefore, only texture changes in beam as well as electric field direction are to be considered, which in terms of, e.g., the tetragonal phase are correlated with a preferred orientation in the crystallographic $[001]_c$ direction. For the rhombohedral phase the $[111]_c$ direction was found to be the preferred orientation. The implementation of this texture model is required to obtain accurate phase fractions.

As the domain structure of unpoled samples at the MPB consists of a combination of tetragonal microdomains and nanodomains,[8] a two-phase Rietveld fit was applied. If nanodomain structures are present, their internal structure is averaged by coherence effects in diffraction to a *Cm* phase with
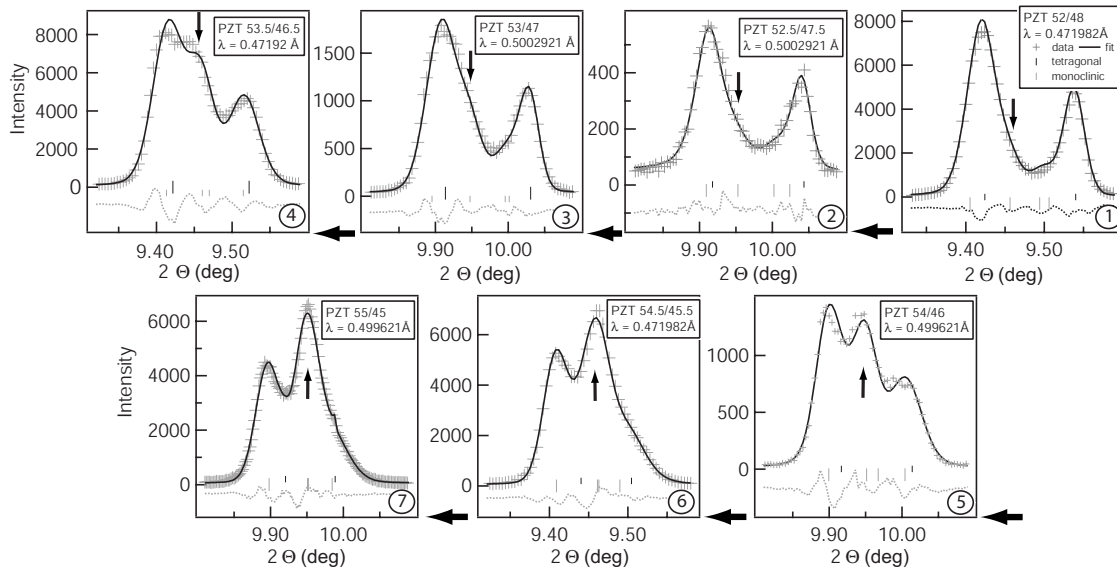
FIG. 2. Rietveld fit depicting the variation in shape and intensity of the tetragonal $101_T/110_T$ reflection pair (vertical arrows) with increasing Zr content in the unpoled state, starting with PZT 52/48 up to PZT 55/45 (horizontal arrows) using high-resolution synchrotron powder diffraction.

a pseudocubic c/a-ratio larger than 1.[6,9,10] Furthermore, internal strain and coherence effects between domains can cause anisotropic broadening effects of certain reflections. Samples of a higher Zr content and an internal rhombohedral symmetry are therefore best fitted using a monoclinic *Cm* model as long as no model for an adequate description of the real structure has been proposed for Rietveld analysis. The resulting lattice parameters for a rhombohedral phase, recalculated from a monoclinic fit to pseudocubic axes, have a c/a-ratio of ~1. This way the content of tetragonal microdomains and nanodomains or rhombohedral microdomains in the sample can be estimated[9] using a tetragonal *P4mm* and a monoclinic *Cm* phase in the Rietveld fit to monitor changes in lattice parameters and phase fraction under varying electric field. The changes in monoclinic c/a-ratio allow a differentiation between nanodomain structures and rhombohedral microdomains.

III. RESULTS

A. High-resolution powder diffraction of the unpoled state

Before investigating the reaction of the series of samples to an applied electric field, the unpoled state is described and will function as a basis for further analysis: In earlier work on material of higher sintering temperature (1225 °C) we have been able to show that the average domain structure miniaturizes at the MPB and that beside tetragonal microdomains nanodomain structures are present,[8] which can be correlated with the observation of a monoclinic phase in diffraction.[6,9,10] A model derived from martensitic theory is applied,[6,9,13] where the intensity, which can be fitted using monoclinic symmetry, is seen as an average over nanodomain structures. The phase fraction of nanodomains present beside tetragonal microdomains can therefore be determined using a two-phase Rietveld fit of a *P4mm* and a *Cm* symmetry.

High-resolution synchrotron x-ray powder diffraction on the series of samples used for *in situ* investigations depict similar properties as their counterpart of higher sintering temperature. Observations in diffraction show a gain in intensity in the angular range between the tetragonal $101_T/110_T$ reflections and in asymmetry of the 101_T with respect to single phase tetragonal samples. The gain is visible in Fig. 2 indicated by vertical arrows, evolving into an additional peak with increasing Zr content (Fig. 2 with increasing number). By lacking an additional 002_R peak this intensity can be attributed to the presence of nanodomains. Furthermore, the asymmetry between $002_T/200_T$ increases with increasing Zr content. As seen in Fig. 3 the changes in nanodomain fraction with decreasing Ti content–represented by the monoclinic phase fraction with a c/a-ratio larger than 1–go along with a decrease in tetragonal and monoclinic c/a-ratio.
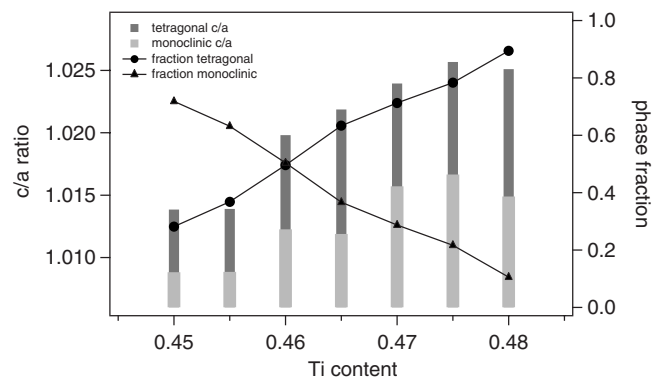
FIG. 3. Phase fractions and c/a-ratio derived from two-phase Rietveld refinement of high-resolution synchrotron powder diffraction data.

B. Macroscopic strain

Marked features of the strain cycles of all morphotropic undoped PZT materials depicted in Fig. 4 are low compressive strain when cycling them with fields inverse to the actual poling direction below the coercive field E_c. In contrast to donor doped materials with a distinct E_c, the changeover to a positive field induced strain is extended over a wider range of electric field. The first effect points toward a low degree of remanent strain. The latter indicates that the activation of microscopic mechanisms, which are providing strain, are distributed over a wide field range. There are, however, considerable differences depending on composition. Samples close to the tetragonal single phase region as PZT 52/48 show a very sluggish transition toward positive strain vs electric field (S-E) characteristics, which occurs only for fields of more than 2 kV/mm. The strain at 4 kV/mm is below 0.1%. Almost no compressive strain was recorded for these materials. For PZT 53/47 similar strain behavior was found. The aforementioned strain characteristics are, however, less pronounced compared to PZT 52/48. In contrast to that, for compositions with higher Zr/Ti ratios the "switching" to positive S-E characteristics occurs at much lower fields (e.g., 0.5 kV/mm for PZT 55/45). A large part of the reaction under electric field seems to be completed within a 0.5 kV/mm field range, as can be seen from the strain curve which is turning into an approximately linear behavior at 1 kV/mm for PZT 55/45. The strain in this sample at the maximum field of 4 kV/mm is 0.19%, thus, almost twice as high as for PZT 52/48. There is clear evidence for compressive strain at fields inverse to the actual poling direction in this sample, although it is at levels below 0.05% only. The strains in PZT 54/46 and PZT 56/44 show qualitatively similar features as for PZT 55/45, though they are quantitatively different.

Summarizing the results from the strain measurements, the general strain behavior in the undoped samples is similar to that of acceptor doped materials. In undoped material at the MPB with high Ti content, the strain response to electric fields is hindered and only detectable at high values of the electric field. Increasing the Zr content and crossing the MPB, strain is higher and occurs at much lower electric fields. Moreover, the compressive strain in these samples indicates the presence of remanent polarization.

Even in the undoped state Fe is present in low abundance as an extrinsic impurity, however, amounts are too low to significantly influence domain or crystallographic structure.[9] In order to understand the influence of acceptor as well as donor doping on the microstructure formed and its reaction to an applied electric field, further studies are currently undertaken. As a first indication it can be said that the amount of nanodomains with La donor doping is increased for samples in the Ti-rich side of the MPB.[41]

C. Changes in intensity and reflection positions under electric field: *In situ* synchrotron x-ray diffraction

In x-ray diffraction measurements both changes in texture and the stretching of unit cells oriented in direction of the electric field can be recorded[19] to directly monitor the micro-
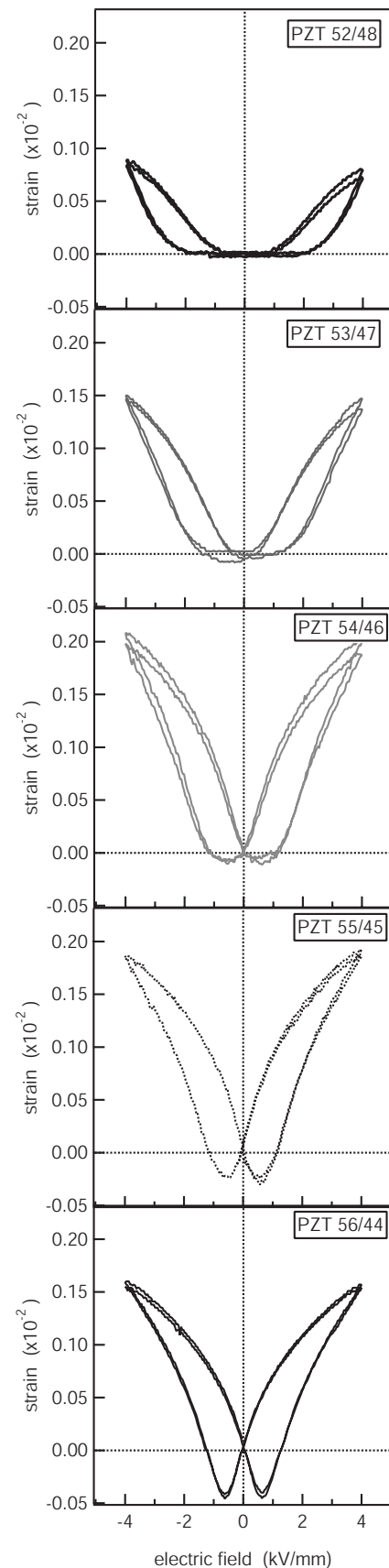
FIG. 4. Macroscopic strain measurements of PZT 52/48 to PZT 56/44. With increasing nanodomain content the strain to an applied electric field increases.
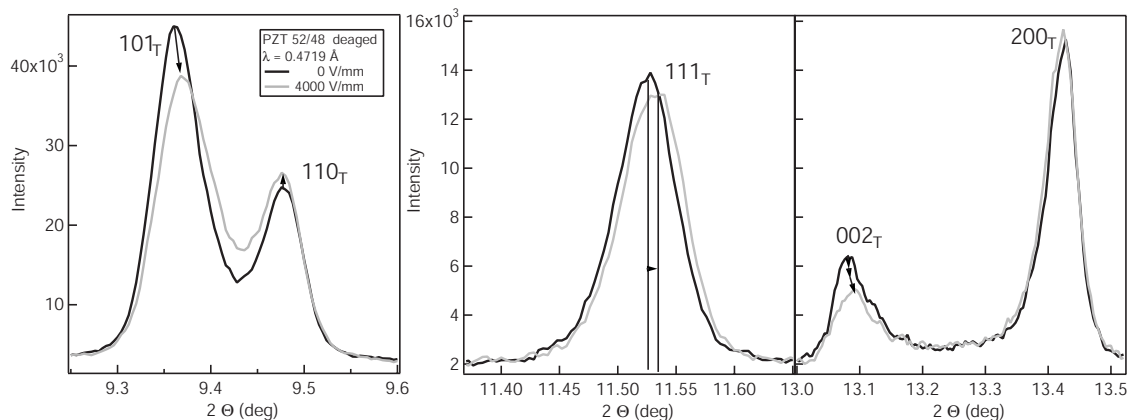
FIG. 5. Diffraction patterns of the tetragonal $101_T/110_T$, 111_T, and $002_T/200_T$ reflections of PZT 52/48, recorded *in situ* under an electric field for the first poling cycle at zero field and at 4 kV/mm deaged by various poling cycles to fully enable a reaction of the material and a stabilization of tetragonal microdomain states.

structural response of PZT. Variation in texture is visible in changes in intensity of reflections and may influence shifts of single peaks, while stretching of the unit cell is only influencing peak positions in single phase samples.

1. PZT 52/48 and PZT 52.5/47.5

In the transmission setup used at beamline B2, texture changes in diffraction patterns of tetragonal samples are seen in, e.g., a decrease in the intensity of the 002_T reflection in Fig. 5. The orientation of domains within the sample is altered, as the material tries to align its macroscopic polarization direction with the direction of the electric field. In general, the way the experiment is set up, no increase in intensity of the $\{00l\}_T$, $\{111\}_T$, and $\{101\}_T$ reflections is observed for tetragonal domain switching. For example, in terms of the tetragonal (002) planes the decrease in intensity results from an alignment of the tetragonal c axes in field direction, and with the x-ray beam and direction of the electric field being parallel, (002) planes are reoriented out of the diffraction condition. The amount of texture can be estimated comparing the difference in intensity ratios before and during poling.

Theoretically a stretching of unit cells in polarization direction should be largest for unit cells with the tetragonal c axis fully or already partially aligned to the electric field. In our setup large shifts in the 111_T and small shifts in the 101_T reflection positions to higher values in 2θ under field are observed, as also reported for 111_T reflections of tetragonal material by Hall *et al.*[22] in their transmission setup, which is similar to our geometry but rotated about 90°. In our data, an elongation of the tetragonal unit cell in direction of the polarization vector is not visible in $\{00l\}_T$ reflections due to experimental restrictions.

In tetragonal samples with compositions in the vicinity of the MPB, changes in reaction to an applied electric field with respect to pure tetragonal samples are observed. With a miniaturization of the average domain structure,[8] not only a decrease in intensity under applied electric field is observed as described above, but between the tetragonal 101_T and 110_T reflections intensity also starts to increase at high electric

fields. In PZT 52/48 and PZT 52.5/47.5 this increase is small, and is just taking place above 2 kV/mm. Other reflections show intensity changes equivalent to tetragonal domain switching. Intensities fall back to starting values when the field is removed. This conforms with macroscopic strain measurements, which indicate that after removing the field the strain falls back to its initial state (Fig. 4).

2. PZT 53/47 and PZT 53.5/46.5

In PZT 53/47 the increase in intensity between the tetragonal 101_T and 110_T reflections in the unpoled state with respect to single phase tetragonal material (Figs. 2 and 3) is quite pronounced and the phase fraction of nanodomains is around 30%. Under the first application of an electric field it develops into a new peak above 2.5 kV/mm (Fig. 6, B1). The 111_T shifts to higher values in 2θ, but furthermore a shoulder develops out of the asymmetry at lower 2θ angles, which remains present but decreases in intensity with higher voltage applied (Fig. 6, B2). The positions of the 002_T and 200_T reflections (Fig. 6, B3) both shift strongly to smaller tetragonality and decrease in intensity. An increase in intensity next to the 200_T is observed which goes along with the large gain in intensity between the 101_T and 110_T reflections. This new reflection between 101_T and 110_T is stable on the downward branch of the hysteresis after poling the sample with up to +4 kV/mm, showing remanence at zero field. It vanishes on the negative branch of the hysteresis at the negative coercive field around −1.5 kV/mm before increasing again with larger fields down to the negative absolute value of −4 kV/mm. Changes in PZT 53.5/46.5 are very similar to PZT 53/47. At zero field the nanodomain content is already larger with approximately 40% and the intensity between 101_T and 110_T is already observable as a separate reflection (Figs. 2 and 4). Under field an increase in the intensity of this reflection is observed from 2.0 kV/mm on. If the downward and negative cycle is considered, coercive field can be determined to be about ±1.0–1.5 kV/mm. The reflection stays present under electric field.

3. PZT 54/46 and PZT 54.5/45.5

For PZT 54/46 and PZT 54.5/45.5 samples a distinct peak between 101_T and 110_T is already present at zero field
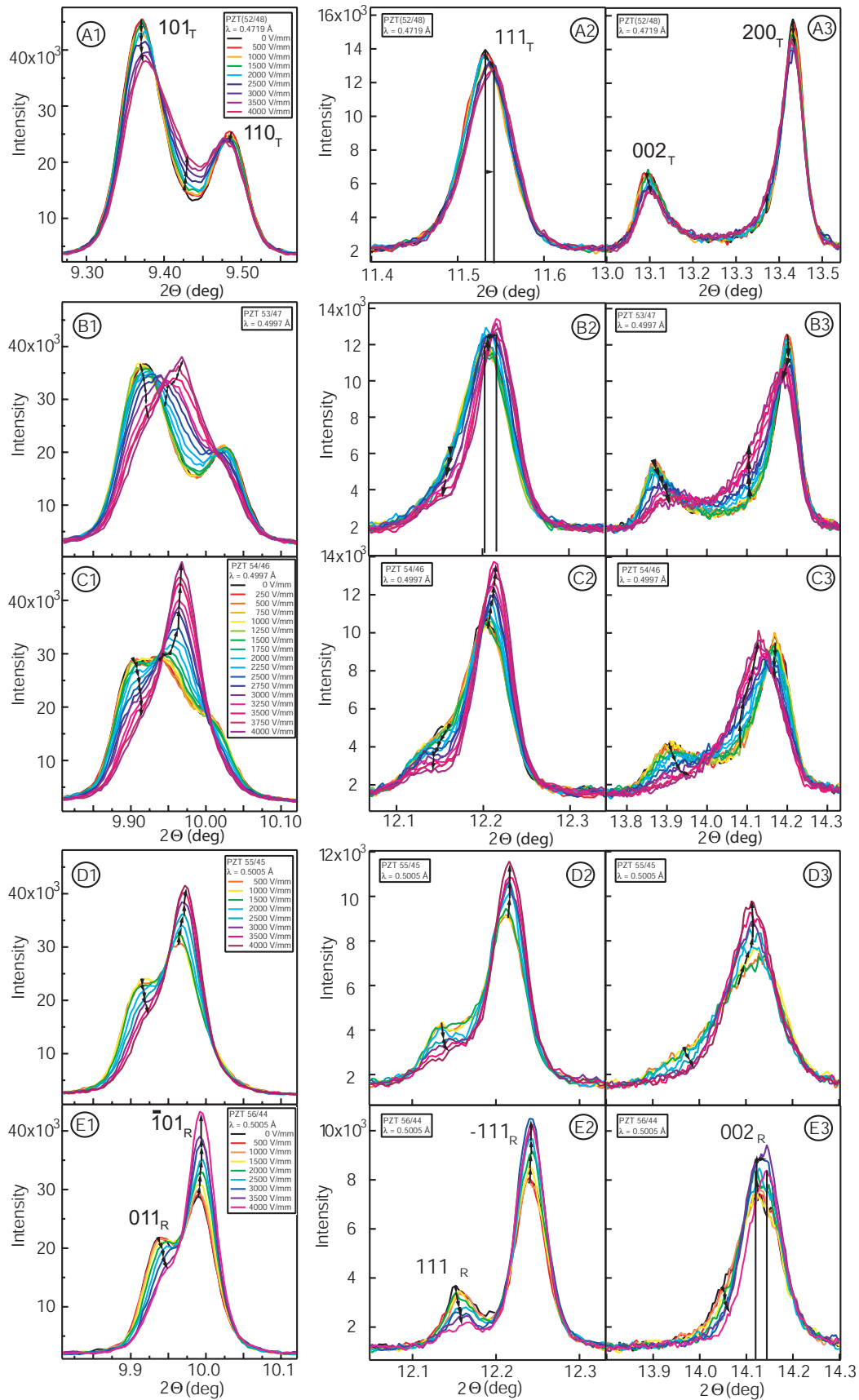
FIG. 6. (Color) Diffraction patterns of the tetragonal $101_T/110_T$ and $002_T/200_T$ reflection pairs of PZT 52/48, PZT 53/47, PZT 54/46, PZT 55/45, and PZT 56/44 recorded *in situ* under an electric field for the first poling cycle of up to 4 kV/mm.
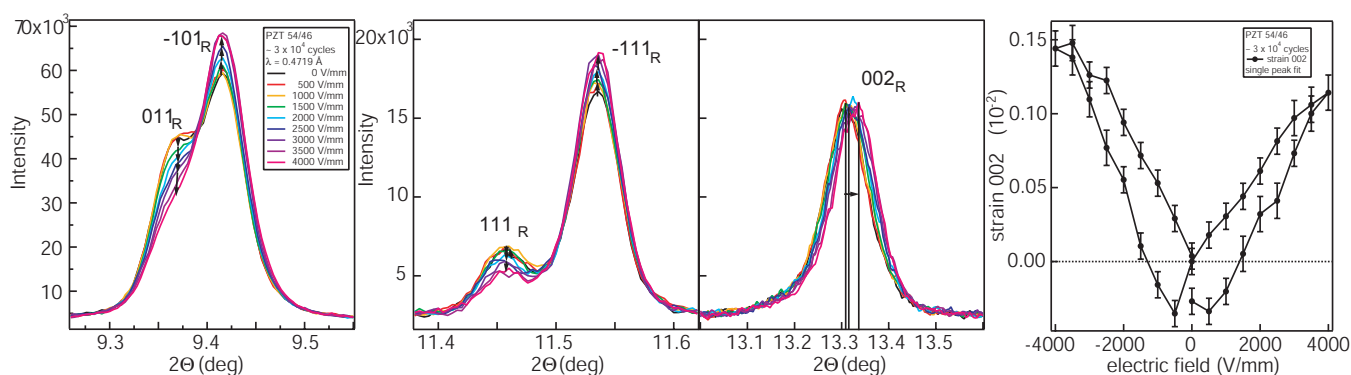
FIG. 7. (Color) Diffraction patterns of the rhombohedral $011_R/\bar{1}01_R$, $111_R/\bar{1}11_R$, and 002_R reflection pairs of PZT 54/46, *in situ* under an electric field in an unfatigued state after 3×10^4 poling cycles of up to 4 kV/mm. Changes characteristic of rhombohedral material as the shift in 002_R and the changes in intensity ratios in $111_R/\bar{1}11_R$ and $011_R/\bar{1}01_R$ are observed. The shift of 002_R extracted by single peak fits show the high intrinsic response of the material.

(Figs. 2, 5, and 6). While the absence of a rhombohedral 002_R reflection between 002_T and 200_T in PZT 54/46 indicates that no coexistence of tetragonal and rhombohedral microdomains but of tetragonal microdomains and a nanodomain structure is present, this distinction in PZT 54.5/45.5 already is difficult, as peaks overlap due to a small tetragonal c/a-ratio. The nanodomain fraction for both materials ranges between 50% and 60% (Fig. 3).

Changes under electric field are most pronounced for PZT 54/46, while the reaction of PZT 54.5/45.5 is very similar and will therefore not be described in detail: The increase in intensity in the additional reflection between 101_T and 110_T is drastic, starting at an applied field of 1.25 kV/mm in the first cycle (Fig. 6, C1). The 002_T and 200_T shift to very small c/a-ratios, both decreasing in intensity, while an additional increase in intensity evolving into a new peak next to the 002_T reflection is observed (Fig. 6, C3). The pattern changes permanently, as it is converted into one similar to the diffraction patterns of samples with higher Zr content containing rhombohedral microdomains as PZT 56/44, which will be described in detail later. The behavior of the pseudocubic $\{111\}_c$ is similar to that in PZT 53/47; however, the intensity gain and loss, as well as the splitting, is larger under electric field (Fig. 6, C2).

After the first poling cycle, at the negative coercive field around -1.25 kV/mm the intensity of the new $\bar{1}01_R$ reflection decreases again, but does not reach starting values again as in PZT 53/47. After a larger number of cycles changes can completely be classified as equivalent to rhombohedral switching, as can be seen in intensity changes and peak shifts in Fig. 7. Texture changes are visible in the split 111_R and $\bar{1}11_R$ reflection pair without shift of reflection positions, while the 200_R shifts to higher diffraction angles. Intensity is gained in the $\bar{1}01_R$ reflection and a decrease and a small shift to higher 2θ values of the 011_R reflection is observed.

4. PZT 55/45 and samples with higher Zr content

In PZT 55/45 and PZT 56/44 the morphotropic diffraction pattern, with its split pseudocubic $\{111\}_c$ and $\{200\}_c$ reflection groups, changes into a single phase rhombohedral

pattern upon first poling (Fig. 6, D and E) with a single symmetric 200_R and a split 111_R and $\bar{1}11_R$ reflection pair. Intensity changes in the pseudocubic $\{101\}_c$ reflections are equivalent to those visible for rhombohedral samples with higher Zr content, as described above for PZT 54/46 after a larger number of cycles.

PZT 57.5/42.5 contains only rhombohedral microdomains[36] and, therefore, shows classical rhombohedral domain switching from the first application of field on.

D. Rietveld refinement of *in situ* data: Changes in phase content and lattice

Using Rietveld refinement the changes in phase content and domain configuration under electric field can be estimated.

In single phase samples containing rhombohedral or tetragonal microdomains, only changes in texture can be determined using Rietveld refinement by the evaluation in changes of preferred orientation and peak width. Shifts of single peaks caused by intrinsic strain effects as presented above for, e.g., the 111_T reflection (Fig. 6, A2), however, have to be analyzed using single peak fits, as Rietveld refinement can solely account for larger changes in the entire lattice and not for different stretching of cells with respect to their orientation to the field direction. In the single phase samples at the edge of the MPB–as PZT 57.5/42.5 (Fig. 8) and PZT 52/48–therefore only marginal changes in average lattice parameters are observed, whereas significant changes in preferred orientation are calculated. Hence, classical tetragonal or rhombohedral domain switching results only in small changes in lattice parameters in Rietveld refinement under the application of an electric field, while the shifts in individual reflections cannot be accounted for. A hysteresis in the change of the 002 lattice plane distances in PZT 57.5/42.5 can be deduced from the change in the monoclinic c axis (Fig. 8); however, to get a more accurate account of the behavior single peak fits of the 002_R would be required.

In PZT 52/48 texture effects are modeled using the tetragonal [001] direction for March-Dollase preferred orientation, as also depicted for PZT 53/47 in Fig. 9. The tetragonal
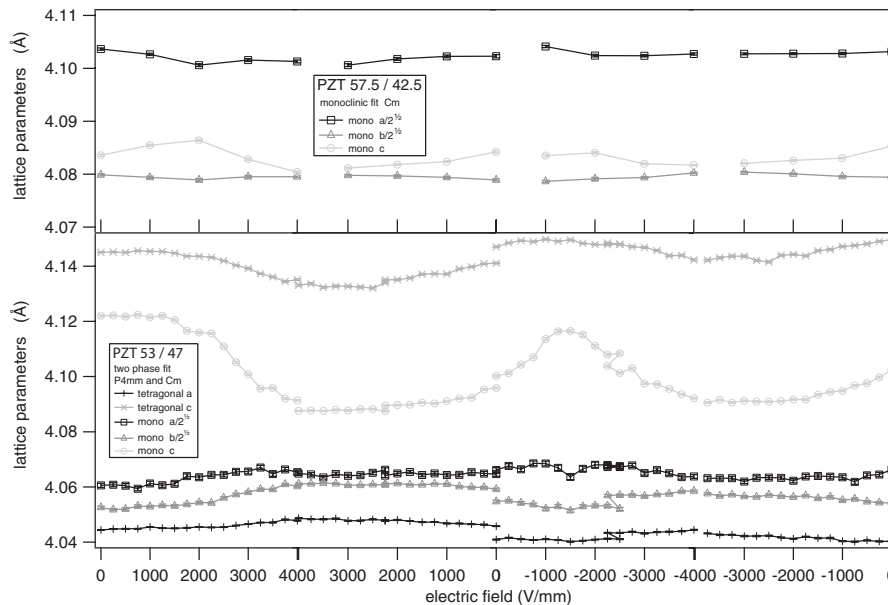
FIG. 8. Changes in lattice parameters in rhombohedral PZT 57.5/42.5 and PZT 53/47 of morphotropic composition under an electric field of up to 4 kV/mm extracted from Rietveld fits.

domains are oriented in field direction changing intensity ratios as described above. In PZT 57.5/42.5 predominantly a decrease in intensity for the rhombohedral 011_R and 111_R is observed, the lattice directions perpendicular to these plains were chosen as preferred orientation directions for March-Dollase modeling. In Rietveld, the change in intensity of 111_R is monitored in the preferred orientation ratio, while the change in intensity of 011_R goes along with changes in peak width and therefore alters the anisotropic peak broadening parameter in this direction. All other Stephens parameters remain constant throughout the refinement although left variable.

As we approach the compositional range between PZT 52.5/47.5 and PZT 56/44, in which a nanodomain structure is present in the unpoled state, strain balances seem to change drastically under electric field. We will focus on the results for PZT 53/47 and PZT 54/46, as the changes with varying nanodomain content are most pronounced and these samples can function as model systems for the differences observed.

In PZT 53/47 phase contents of 60% tetragonal microdomains and 40% nanodomain structures derived from fits of image-plate data of the unpoled state are present. Lattice parameters of this material derived from Rietveld refinement start to vary strongly with electric field (Fig. 8) and a decrease in c/a-ratio in both the tetragonal and the monoclinic fits (Fig. 10) is observed in the direction perpendicular to the electric field. Phase fractions alternate around an average value with varying applied field and texture in the tetragonal phase increases in correspondence to a decrease in tetragonal phase content (Fig. 9).

PZT 54/46 contains an initial *ex situ* fraction of 45% tetragonal microdomains and 55% nanodomains. In the beginning of the first poling process also a strong change in both lattice parameters and c/a-ratio of the two-phase models are detected. However, while the decrease in tetragonal

c/a-ratio in PZT 53/47 recovers close to the negative coercive field, as seen in the variations in c/a-ratio in Fig. 10, with a more or less stable variation in phase fractions over the entire cycle, in PZT 54/46 the content of tetragonal microdomains decreases drastically down to around 10%, never to recover again. While in PZT 53/47 the tetragonal lattice parameters show a hysteresis under applied field, the c/a-ratio of the tetragonal phase in PZT 54/46 is not well defined, mainly due to the small value of the phase fraction. Lattice parameters calculated based on the monoclinic fit show a much smaller c/a-ratio in PZT 54/46 with smaller variations than in PZT 53/47. The hysteresis is more pronounced in PZT 53/47; however, in both samples the values of the monoclinic c/a-ratio approach 1 under electric field, equivalent to the values derived for a rhombohedral microdomain structure.[9]

In PZT 55/45 and PZT 56/44 the phase fractions of tetragonal microdomains and the c/a-ratio of this phase are even smaller so that a transition to a fully rhombohedral structure showing rhombohedral domain switching after the first poling process requires lower electric fields than in PZT 54/46.

IV. DISCUSSION

Before discussing the effect of the electric field, we have to account for the variation in phase fractions obtained by Rietveld fits of high-resolution data and image-plate data. The values vary slightly, which again underlines the model assumption that the monoclinic phase fitted is a result of coherence effects between nanodomain structures.[6,9,10] Therefore, only absolute values for phase fractions derived from data recorded under equivalent conditions are comparable. Trends within a series of recordings, however, are equivalent.
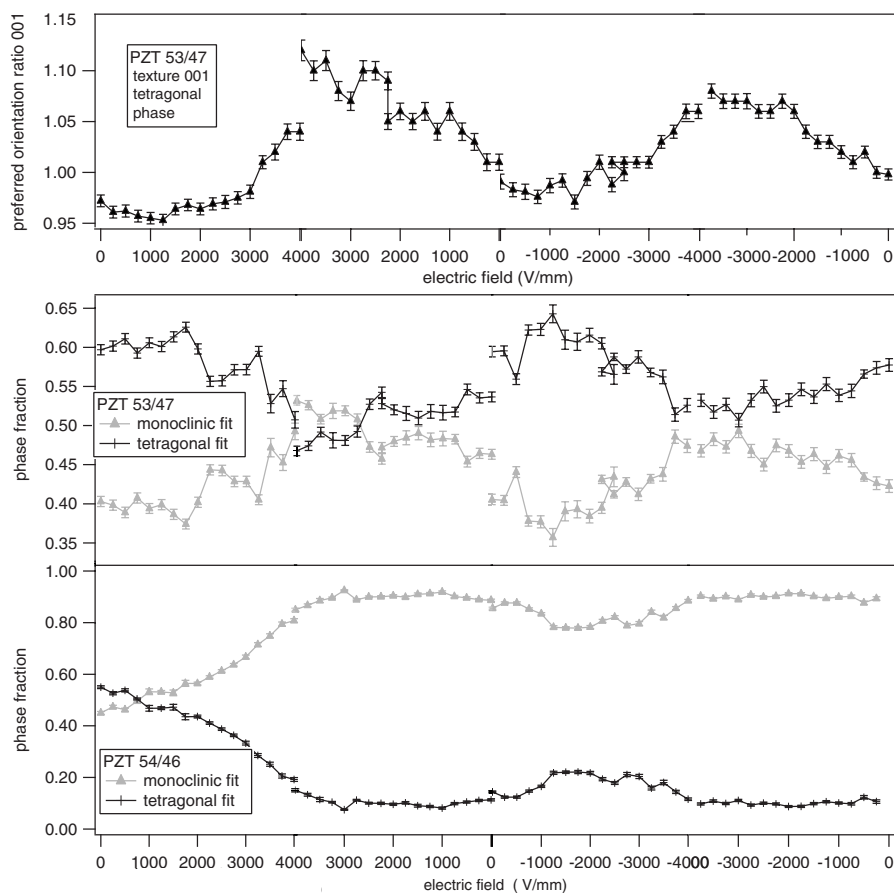
FIG. 9. Changes in texture in the tetragonal phase of PZT 53/47 as well as in phase fractions under an electric field of up to 4 kV/mm in PZT 53/47 and PZT 54/46 derived from Rietveld fit.

The behavior of the complex domain structure at the morphotropic phase boundary in PZT has a major influence on the reaction of the material to an applied electric field. While on the single phase side of the MPB, with tetragonal or rhombohedral symmetry, reversible domain switching processes are observed, the samples of morphotropic composition show various pronounced changes in the structure, which are reversible only under a distinct balance between nanodomain content and tetragonal c/a-ratio. This is now specified in more detail.

In samples with a Zr content higher than PZT 53.5/46.5 a transition from a structure consisting of tetragonal microdomains and nanodomains to one of rhombohedral microdomains takes place. In these samples the c/a-ratio is already small and the nanodomains are forced to collapse into rhombohedral microdomains under the first application of an electric field. In contrast to PZT 55/45 and PZT 56/44, the complete transition in domain and crystal structure in PZT 54/46 and PZT 54.5/45.5 requires more than one cycle. At the negative coercive field of the first poling cycle, a nanodomain structure is partially recovered, as seen in the hysteretic variation of the monoclinic c/a-ratio in Fig. 10. However, starting values are never reached again and the low values in c/a-ratio under high electric field are clearly correlated to a rhombohedral structure, as they are around 1.[9] There are only marginal changes and a lot of scatter in the tetragonal c/a-ratio. This is attributed to a decrease in tetrag-

onal phase fraction down to about 10%, which only partially recovers to 20% at the negative coercive field in the first cycle. It has to be kept in mind that the undoped samples are all aged, signifying that domain walls may be pinned and a *P-E* hysteresis loop is constricted before defect structures can be mobilized by the field. With increasing number of electric cycles, the samples can be deaged and the fraction of nanodomains, that was recovered in the first cycles at the negative E_c after poling with a positive voltage, vanishes, seen for PZT 54/46 in Fig. 7 after $\sim 3 \times 10^3$ cycles. The sample depicts rhombohedral switching and large intrinsic strain seen in the large variation of the 002 reflection. This behavior shows that the nanodomain structures are not stable under electric field in undoped PZT samples of small tetragonal c/a-ratio before application of an electric field.

Samples with large c/a-ratio but still high enough Zr content to form nanostructures such as PZT 53/47 and PZT 53.5/46.5 display an ambiguous behavior under electric field. They settle in between samples undergoing a rhombohedral phase transition (PZT 54/46) and samples such as PZT 52.5/47.5, which assemble into tetragonal microdomains after several cycles. The tetragonal c/a-ratio in PZT 53/47 seems large enough to form a counterweight to the tendency of the nanodomains to form larger rhombohedral structures under applied field. The fraction of tetragonal microdomains and nanodomains under electric field alternates around 50% and the nanostructures remain stable even with
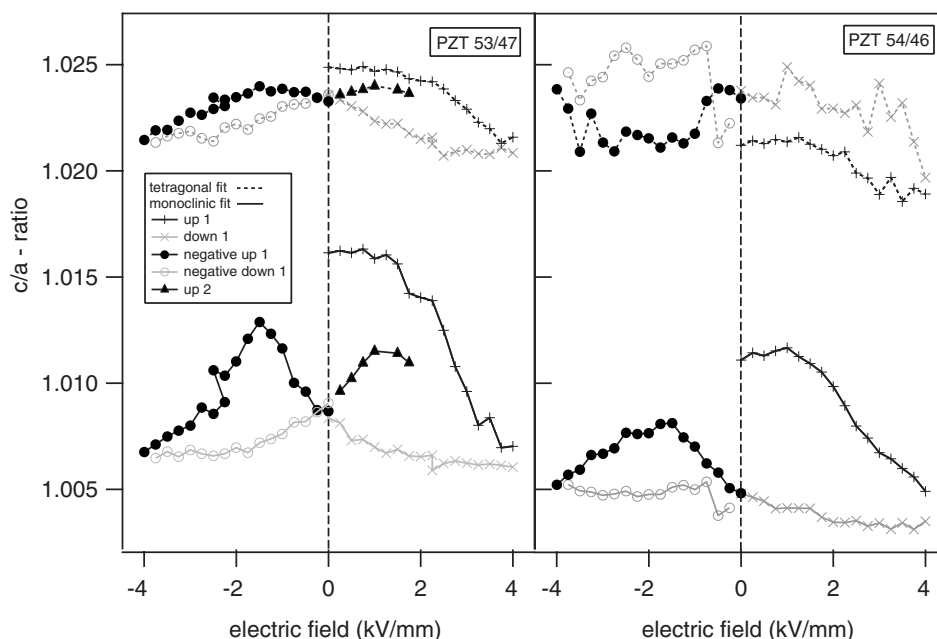
FIG. 10. Hysteresis of the changes in c/a-ratio of the tetragonal and monoclinic phases derived from Rietveld fits of PZT 53/47 and PZT 54/46.

an increasing number of cycles. While at high electric fields the nanodomains rearrange into rhombohedral microdomains, the tetragonal unit cells oriented perpendicular to the electric field direction are compressed along their c axis (Figs. 8 and 10). It is unclear whether phase fractions remain constant under field or whether the tetragonal microdomains are transformed into nanodomains, as the tetragonal microdomains are reoriented out of the diffraction condition and into field direction parallel to the x-ray beam thus reducing their scattering volume as implied by the changes in preferred orientation. Observed changes in domain configurations are similar to the results from *in situ* conditions in transmission electron microscopy studies of commercial PZT by Tan *et al.*,[37] where under high electric fields nanostructures are arranged into larger domains.

The macroscopic strain behavior of the materials seems to mirror these changes observed by diffraction (Fig. 4). In undoped material with predominantly tetragonal microdomains, the strain response to electric fields is hindered and only detectable at high values of the electric field. In the samples in which considerable fractions of nanodomains were detected before application of an electric field, strain is higher and occurs at much lower electric fields. Moreover, the compressive strain in these samples indicates the presence of remanent polarization.

Nanodomain structures and the observation of a monoclinic phase in diffraction are directly correlated. Highest macroscopic strain values in the first poling cycles in undoped samples are observed for PZT 54/46 and PZT 54.5/45.5, which both change from a structure showing a diffraction pattern formerly attributed to monoclinic symmetry into a rhombohedral material on first poling. Furthermore, PZT 54/46 in the rhombohedral phase shows a large 002_R shift attributed to intrinsic strain under electric field

(Fig. 7). High intrinsic strain in single phase material close to the MPB as PZT 60/40 was predicted by large calculated d_{15} shear values.[38] On poling we can say that no stable monoclinic phase is present in these samples of high nanodomain content and observed high coherence effects in diffraction before application of an electric field. So for these samples the model assumption that a high piezoelectric response in morphotropic PZT is linked to a polarization rotation within one plane of a single unit cell of a stable monoclinic phase[4,5,39] cannot be verified. Jin *et al.*[6] and Wang[40] have pointed out that a macroscopic rotation of the polarization can be achieved through redistribution of the orientation of nanodomain structures without changing the crystallographic structure of the system. This indicates that a low domain wall energy and therefore high domain and domain wall mobility may strongly influence macroscopic properties. The processes present in materials containing stable nanodomain states (PZT 53/47 and PZT 53.5/46.5) which transform into larger rhombohedral microdomains under the influence of an electric field may be an example for this behavior, which, however, requires further investigation as, e.g., through *in situ* TEM studies under an electric field.[41] The nanodomain structure present and the ability of the material to undergo phase transitions under electric field may be linked to the flattening of the Gibbs free energy profile on both sides of the MPB with respect to single phase material described by Budimir *et al.*[42] In samples at the MPB with higher Ti content these internal properties might be triggering the formation and rearrangement of domain configurations.

If we discuss the observed reaction of the structure of PZT with respect to recent postulations about the origin of high piezoelectric strain within the material at the MPB, it can be stated that, considering the transition behavior observed, the most likely model applicable to the behavior of

PZT is the reorientability of nanodomain structures due to a low domain wall energy[6] and complete transitions showing high intrinsic strain, depending on composition. The recent model on domain wall broadening inducing, e.g., a rhombohedral symmetry within tetragonal domains proposed by Rao and Wang[7] cannot be confirmed for samples on the tetragonal side of the MPB using diffraction. However, if we approach a distinct balance between Zr/Ti content and tetragonal distortion as in PZT 53/47, the transitional behavior under electric field from tetragonal microdomains to rhombohedral microdomains via the nanodomain structure straining the tetragonal parent phase, and a lack of stability of the rhombohedral phase after application of the electric field may indicate that the mechanisms postulated cannot be excluded. Our observations, however, can be linked best to the reorientation and stability of nanodomain structures previously described for relaxor material.[6,10] Experimental limitations of diffraction experiments prohibit the observation of a change in domain wall width with nanodomain structures present in the structure at the same time. At the present state of our investigation the crystallographic structure of the nanodomains has not been elucidated yet. The rearrangement of nanodomains into rhombohedral microdomains under electric field derived from diffraction data is a strong hint. Also a very good fit of single phase rhombohedral samples using a monoclinic *Cm* phase supports the assumption that coherence effects play an important role in diffraction of these structures.[9] Consistency is given with calculations based on martensitic theory[6,10,13] that the internal symmetry of nanodomain structures, which appear monoclinic in diffraction, is likely not to be monoclinic and can be proposed as rhombohedral.

V. CONCLUSION

According to our results the behavior of undoped morphotropic PZT under electric field strongly depends on the morphology of the domains and the tetragonal distortion present. It is shown that the reaction of the complex domain structure and resulting structural transitions can be captured and explained using *in situ* synchrotron x-ray diffraction. Various criteria for the reaction of morphotropic material to an electric field can therefore be defined as follows.

(1) With *small nanodomain content* ($\leq 25\%$) and *large tetragonal c/a-ratio* (≥ 1.025) the nanodomains vanish under the application of an electric field and a tetragonal domain structure is stable–as for undoped PZT 52.5/47.5 and for lower Zr content.

(2) With *large nanodomain content* ($\geq 45\%$) and *small tetragonal c/a ratio* (≤ 1.02) a phase transition to rhombohedral microdomains takes place during the first poling cycles, which is not reversible. Only at E_c of the first cycles the domain structure partially miniaturizes again, which falls off with the number of cycles–as in undoped PZT 54/46 and for higher Zr content. After various cycles high intrinsic strain is observed by the shift of the 002_R reflection.

(3) For intermediate parameters (25% $\leq$ nanodomain content $\leq 45\%$, $1.02 \leq$ tetragonal c/a-ratio ≤ 1.025) the nanodomain structures and tetragonal microdomains are both stable under electric field and counterbalance each other. While the nanodomains form rhombohedral microdomains under electric field the tetragonal unit cells are compressed. Changes under electric field are reversible–as for undoped PZT 53/47 and PZT 53.5/46.5. The lattice parameters of the tetragonal phase are altered drastically.

For the first and last case information on texture changes in diffraction can be extracted and evaluated; however, difficulties in interpretation may arise in material with stable nanodomains due to coherence effects. The stabilization of nanodomains enhances the ability of the material to align in an external electric field. Internal strain fields–as seen in large changes in lattice constants and a compression of the tetragonal phase not oriented in direction of the electric field in samples where nanodomains are present beside tetragonal microdomains–are much larger in these materials than in single phase samples and may contribute strongly to the piezoelectric response of the material. The high d_{15} values at the MPB discussed by Damjanovic[38] along nonpolar axes may be enhancing the intrinsic piezoelectric response of each domain and trigger transition processes. The high piezoelectric response may also be influenced by the stability of certain domain sizes and possible coexistence of various domain states. The behavior can be related to models recently proposed for the reorientation of nanodomain structures[6] under electric field and domain wall broadening[7] while a polarization rotation within a stable monoclinic phase could not be verified.

*Author to whom correspondence should be addressed. FAX: +49-6151-166377; schoenau@matgeo.tu-darmstadt.de

[1] B. Jaffe, W. R. Cook, and H. Jaffe, *Piezoelectric Ceramics* (Academic, London, 1971).

[2] M. J. Hoffmann and H. Kungl, Curr. Opin. Solid State Mater. Sci. **8**, 51 (2004).

[3] W. Cao and L. E. Cross, Phys. Rev. B **47**, 4825 (1993).

[4] R. Guo, L. E. Cross, S.-E. Park, B. Noheda, D. E. Cox, and G.

Shirane, Phys. Rev. Lett. **84**, 5423 (2000).

[5] H. Fu and R. E. Cohen, Nature (London) **403**, 281 (2000).

[6] Y. M. Jin, Y. U. Wang, A. G. Khachaturyan, J. F. Li, and D. Viehland, J. Appl. Phys. **94**, 3629 (2003).

[7] W.-F. Rao and Yu U. Wang, Appl. Phys. Lett. **90**, 041915 (2007).

[8] L. A. Schmitt, K. A. Schönau, R. Theissmann, H. Fuess, H. Kungl, and M. J. Hoffmann, J. Appl. Phys. **101**, 074107 (2007).

[9] K. A. Schönau, L. A. Schmitt, M. Knapp, H. Fuess, Rudiger-A. Eichel, H. Kungl, and M. J. Hoffmann, Phys. Rev. B **75**, 184117 (2007).

[10] Y. U. Wang, Phys. Rev. B **73**, 014113 (2006).

[11] H. Boysen, J. Phys.: Condens. Matter **19**, 275206 (2007).

[12] Y. M. Jin, Y. U. Wang, A. G. Khachaturyan, J. F. Li, and D. Viehland, Phys. Rev. Lett. **91**, 197601 (2003).

[13] Yu. U. Wang, Phys. Rev. B **76**, 024108 (2007).

[14] W.-F. Rao and Yu U. Wang, Appl. Phys. Lett. **90**, 182906 (2007).

[15] D. A. Hall, A. Steuwer, B. Cherdhirunkorn, T. Mori, and P. J. Withers, J. Appl. Phys. **96**, 4245 (2004).

[16] G. Arlt and P. Sasko, J. Appl. Phys. **51**, 4956 (1980).

[17] K. S. Lee, Y. K. Kim, and S. Baik, Appl. Phys. Lett. **79**, 2444 (2001).

[18] J. L. Jones, E. B. Slamovich, and K. J. Bowman, J. Appl. Phys. **97**, 034113 (2005).

[19] M. J. Hoffmann, M. Hammer, A. Endriss, and D. C. Lupascu, Acta Mater. **49**, 1301 (2001).

[20] J.-T. Reszat, A. E. Glazournov, and M. J. Hoffmann, J. Eur. Ceram. Soc. **21**, 1349 (2001).

[21] N. Menou, Ch. Muller, I. S. Baturin, V. Ya. Shur, and J.-L. Hodeau, J. Appl. Phys. **97**, 064108 (2005).

[22] D. A. Hall, A. Steuwer, B. Cherdhirunkorn, P. J. Withers, and T. Mori, J. Mech. Phys. Solids **53**, 249 (2005).

[23] M. Liu and K. J. Hsia, J. Am. Ceram. Soc. **88**, 210 (2005).

[24] D. A. Hall, A. Steuwer, B. Cherdhirunkorn, T. Mori, and P. J. Withers, Acta Mater. **54**, 3075 (2006).

[25] W. Chang, A. H. King, and K. J. Bowman, Appl. Phys. Lett. **88**, 242901 (2006).

[26] H. Kungl, R. Theissmann, M. Knapp, C. Baehtz, H. Fuess, S. Wagner, Th. Fett, and M. J. Hoffmann, Acta Mater. **55**, 1849 (2007).

[27] M. Davis, J. Electroceram. **19**, 23 (2007).

[28] M. Hammer and M. J. Hoffmann, J. Am. Ceram. Soc. **81**, 3277 (1998).

[29] S. L. D. Lucato, LINCE 2.31D, TU Darmstadt, FB Materialwissenschaften, FG Nichtmetallisch Anorganische-Werkstoffe.

[30] M. Knapp, C. Baehtz, H. Ehrenberg, and H. Fuess, J. Synchrotron Radiat. **11**, 328 (2004).

[31] M. Knapp, V. Joco, C. Baehtz, H. H. Brecht, A. Berghaeuser, H. Ehrenberg, H. von Seggern, and H. Fuess, Nucl. Instrum. Methods Phys. Res. A **521**, 565 (2004).

[32] A. C. Larson and R. B. von Dreele, Los Alamos National Laboratory, Report (LAUR) 86, 748 (2004).

[33] P. Thompson, D. E. Cox, and J. B. Hastings, J. Appl. Crystallogr. **20**, 79 (1987).

[34] P. W. Stephens, J. Appl. Crystallogr. **27**, 462 (1999).

[35] N. C. Popa, J. Appl. Crystallogr. **25**, 611 (1992).

[36] R. Schierholz, diploma thesis, Darmstadt University of Technology, 2004; (private communication).

[37] X. Tan, H. He, and J.-K. Shang, J. Mater. Res. **20**, 1641 (2005).

[38] D. Damjanovic, J. Am. Ceram. Soc. **88**, 26632676 (2005).

[39] L. Bellaiche, A. García, and D. Vanderbilt, Phys. Rev. B **64**, 060103(R) (2001).

[40] Yu U. Wang, Phys. Rev. B **73**, 014113 (2006).

[41] R. Theissmann, L. A. Schmitt, J. Kling, R. Schierholz, K. A. Schönau, H. Fuess, M. Knapp, H. Kungl, and M. J. Hoffmann, J. Appl. Phys. **102**, 024111 (2007).

[42] M. Budimir, D. Damjanovic, and N. Setter, Phys. Rev. B **73**, 174106 (2006).